

## Solid solution in the celadonite family: The new minerals ferroceldonite, $K_2Fe^{2+}Fe^{3+}Si_8O_{20}(OH)_4$ , and ferroaluminoceldonite, $K_2Fe^{2+}Al_2Si_8O_{20}(OH)_4$

GEJING LI,<sup>1\*</sup> DONALD R. PEACOR,<sup>1</sup> DOUGLAS S. COOMBS,<sup>2</sup> AND YOSUKE KAWACHI<sup>2</sup>

<sup>1</sup>Department of Geological Sciences, The University of Michigan,  
Ann Arbor, Michigan 48109, U.S.A.

<sup>2</sup>Geology Department, University of Otago, P.O. Box 56, Dunedin, New Zealand

### ABSTRACT

Celadonite-family mica minerals occurring in the Triassic Gavenwood Tuffs, Murihiku Supergroup, Hokonui Hills, Southland, New Zealand, have been analyzed by XRD, TEM, AEM, and EMPA. Packets a few unit cells to several hundred nanometers thick are intimately intergrown with chlorite, berthierine, and corrensite. Analyses of homogeneous packets, combined with analyses from the literature, imply complete or nearly complete solid solution between end-members of the celadonite family defined by octahedral exchange involving  $MgFe^{3+}$ ,  $Fe^{2+}Al$ ,  $Fe^{2+}Fe^{3+}$ , and probably  $MgAl$ , and show that EMPA analyses are commonly contaminated by mixtures. Two new minerals of the celadonite family are defined: ferroceldonite,  $K_2Fe^{2+}Fe^{3+}Si_8O_{20}(OH)_4$ , and ferroaluminoceldonite,  $K_2Fe^{2+}Al_2Si_8O_{20}(OH)_4$ . The former occurs largely as submicrometer ( $\leq 200$ – $300$  nm thick) grains in vesicle rims, and the latter admixed with chlorite and mixed-layered minerals in vesicle interiors and replacing glass shards. Heulandite is intimately associated with both ferroceldonite and ferroaluminoceldonite. Both new minerals are blue-green in thin section and occur as 1M polytypes. Powder X-ray diffraction patterns of mixtures show only one set of mica peaks, with only a few peaks exhibiting slight broadening. The strongest lines in the X-ray powder diffraction patterns are [ $d$  ( $l, hkl$ )]: 3.65 (52, 11 $\bar{2}$ ); 3.358 (86, 022); 3.321 (100, 003); 3.090 (60, 112); 2.584 (50, 13 $\bar{1}$ ). A composite sample composed of ferroceldonite and ferroaluminoceldonite gives the following unit-cell data: space group  $C2/m$ ,  $Z = 2$ , with refined average lattice parameters  $a = 5.270(5)$ ,  $b = 9.106(7)$ ,  $c = 10.125(8)$  Å,  $\beta = 100.27$  (14)°,  $V = 478.1(4)$  Å<sup>3</sup>. The calculated densities are 3.045 (3) and 2.928 (2) g/cm<sup>3</sup> for ferroceldonite and ferroaluminoceldonite, respectively. Celadonite mineral-aluminous clay mineral and celadonite mineral-Ca-rich zeolite assemblages of the zeolite facies are related to illite-chlorite  $\pm$  pumpellyite assemblages of higher grade by dehydration reactions, not necessarily under closed-system conditions.

### INTRODUCTION

Celadonite is a dioctahedral mica with the ideal end-member composition  $K_2Mg_2Fe^{3+}Si_8O_{20}(OH)_4$ . Invariably fine-grained and blue-green in color on crushing (celadon green), it has been mined for many centuries as a pigment for porcelains and other purposes from quarries near Verona in Italy (terre verte de Véronne) and in the Troodos massif of Cyprus (Odin et al. 1988). Most recorded celadonites occur in hydrothermally altered mafic volcanic rocks including those from the oceanic crust (e.g., Andrews 1980). Honda and Muffler (1970) described celadonite in altered rhyolitic detritus in an active hydrothermal system spanning temperatures from 80 to 170 °C at Yellowstone National Park, and Cathelineau and Izquierdo (1988) reported it in andesites in the Los Azufres,

Mexico, geothermal system at a temperature inferred from fluid inclusion studies to be  $240 \pm 10$  °C.

Celadonite also occurs in sedimentary rocks, especially those with a tuffaceous or other significant volcanogenic component, as in many Late Paleozoic to Tertiary accretionary complexes. In these it formed under diagenetic or very low-grade metamorphic conditions (Coombs 1954; Wise and Eugster 1964; Boles and Coombs 1975) corresponding to the zeolite facies and less commonly to the prehnite-pumpellyite and lawsonite-albite-chlorite facies (Landis 1974), but it is unknown in the greenschist facies (e.g., Wise and Eugster 1964).

In thin section, celadonite is conspicuous as bright blue-green, fine-grained aggregates in veinlets and vesicles, as botryoids in intergranular void space, and as replacements of other minerals such as hypersthene, olivine, pyroxene, and plagioclase (Hendricks and Ross 1941; Wise and Eugster 1964; Foster 1969; Honda and Muffler 1970; Andrews 1980; Cathelineau and Izquierdo

\* Present address: Department of Geology, Arizona State University, P.O. Box 871404, Tempe, Arizona 85287-1404, U.S.A.

1988; Odin et al. 1988). Transmission electron microscopy (TEM) and analytical electron microscope (AEM) data demonstrate that submicrometer mixed layering is common in fine-grained phyllosilicates formed at low grades (Peacor 1992), and such mixed layering is expected to occur with members of the celadonite family. The celadonite X-ray powder diffraction (XRD) pattern consistently displays reflections corresponding to the 1M mica polytype (Yoder and Eugster 1955; Wise and Eugster 1964; Buckley et al. 1978; Andrews 1980; Odom 1984; Odin et al. 1988). However, powder XRD data are commonly complicated by the presence of intimately intergrown minerals, some of which are also 2:1 phyllosilicates (Hendricks and Ross 1941; Andrews 1980; Loveland and Bendelow 1984; Odin et al. 1988). Optical properties derived from aggregates that may include other phyllosilicates are frequently only approximations to those of celadonite, and electron microprobe analyses of such material commonly include intergrown phases (Li et al. 1996).

End-member celadonite and the end-member  $\text{Fe}^{2+}\text{Fe}^{3+}$  analogue have been synthesized by Wise and Eugster (1964), but attempts by these authors to synthesize the Al end-members were not successful. Velde (1972) reported syntheses with substantial solid solution between the  $\text{MgFe}^{3+}$  and  $\text{Fe}^{2+}\text{Fe}^{3+}$  end-members and much more limited substitution of  $\text{MgAl}$  for  $\text{MgFe}^{3+}$ . The above syntheses were conducted at temperatures of about 300–430 °C and (mostly) 2 kbar fluid pressure and were mostly unreversed experiments. They do not provide definitive information on possible solid solution and stability relationships at the lower temperatures of the zeolite and prehnite-pumpellyite facies.

Boles and Coombs (1975) obtained electron microprobe analyses of celadonitic minerals occurring in altered crystal-vitric tuffs from the Hokonui Hills, Southland, New Zealand, suggesting substantial solid solution but with probable contamination from intergrown chlorite. To determine the compositions of the pure minerals as distinct from mixtures, we have re-analyzed one of the Hokonui Hills specimens using TEM and AEM. The results reveal a broad range of solid solution among the celadonite-family components  $\text{K}_2\text{Mg}_2\text{Fe}_2^{3+}\text{Si}_8\text{O}_{20}(\text{OH})_4$  (celadonite),  $\text{K}_2\text{Mg}_2\text{Al}_2\text{Si}_8\text{O}_{20}(\text{OH})_4$ ,  $\text{K}_2\text{Fe}_2\text{Fe}_2^{3+}\text{Si}_8\text{O}_{20}(\text{OH})_4$ , and  $\text{K}_2\text{Fe}_2^{3+}\text{Al}_2\text{Si}_8\text{O}_{20}(\text{OH})_4$ . Schaller (1950) suggested that an old name, leucophyllite, be applied to micas of end-member composition  $\text{K}_2\text{Mg}_2\text{Al}_2\text{Si}_8\text{O}_{20}(\text{OH})_4$ . With an alkali content of only 3.39%  $\text{K}_2\text{O}$  and 1.42%  $\text{Na}_2\text{O}$ , the analysis on which this suggestion was based is likely to be from a mixture. Schaller's proposal has not achieved acceptance, and celadonite itself was the only one of four end-members that had been accepted as a valid mineral species. The data of our current study allow characterization of the new minerals ferroceldonite,  $\text{K}_2\text{Fe}_2\text{Fe}_2^{3+}\text{Si}_8\text{O}_{20}(\text{OH})_4$ , and ferroaluminoceldonite,  $\text{K}_2\text{Fe}_2^{3+}\text{Al}_2\text{Si}_8\text{O}_{20}(\text{OH})_4$ . The new minerals and names have been approved by the Commission on New Minerals and Mineral Names, International Mineralogical Association. Type material has been de-

posited in the National Museum of Natural History, the University of Michigan, and the Geology Department, University of Otago (OU 26049).

#### OCCURRENCE AND ASSOCIATED MINERALS

The sample used in this study (OU 26049) is an altered crystal-vitric tuff from the Gavenwood Tuffs (early Triassic marine, Murihiku Supergroup), grid reference E45 649657, Hokonui Hills, Southland, New Zealand. Microprobe analyses of heulandite, plagioclase clasts, and celadonite in this rock were reported by Boles (1972) and Boles and Coombs (1975). Broken surfaces of the hand specimen are dark greyish-green in color with reddish flecks and show feldspar clasts up to about 1 mm in length. Larger dark clasts, 1–3 mm in diameter, prove in thin section to be micropumiceous shards and lapilli. Vitroclastic texture is well developed, with cusped shards typically 0.2–0.6 mm in length. Glass in the cusped shards and much of that in the pumiceous lapilli has been replaced by fibrolamellar or platy Ca- and Si-rich heulandite; the interior of the shards commonly is pigmented red or yellow. Heulandite also occupies some of the microvesicles. Celadonite-family materials fill clusters of microvesicles and partially replace glass in the pumiceous shards, collectively forming dark blue-green patches. Vesicles are commonly zoned with a film of celadonite-family mineral lining the rims and larger celadonitic flakes admixed with chlorite in the centers. Some vesicles are filled only with chlorite, and chlorite also occurs in the matrix. Color ranges from bright glaucous-green celadonite through olive-green to pale-green chlorite. TEM studies reveal that mixed-layer chlorite-berthierine and chlorite-corrensite are intimately intergrown with the chlorite host. Other authigenic minerals include titanite as a dusting of micrometer-sized granules, minor pyrite and quartz, localized fine-grained twinned albite, and rare prehnite. Rare siderite of composition  $(\text{Fe}_{0.76}\text{Mn}_{0.10}\text{Mg}_{0.01}\text{Ca}_{0.13})\text{CO}_3$  occupies solution cavities in former glass shards and microfractures in the matrix. Abundant detrital plagioclase, zoned and ranging from labradorite to oligoclase, is accompanied by lesser amounts of augite, magnetite, and rare hornblende. Quartz and biotite are very sparse. There are also scattered lithic volcanic fragments of andesitic to rhyolitic composition.

#### METHODS

The XRD data were obtained for < 0.2  $\mu\text{m}$  separates (obtained by settling in a water column), using a Philips automated diffractometer with graphite monochromator and  $\text{CuK}\alpha$  radiation (35 kV and 15 mA) with quartz as an internal standard. A step size of 0.02  $2\theta$  and a long counting time of 6 s per step were used, the latter to increase resolution of weak peaks.

Polished epoxy and sticky wax-backed thin sections were prepared for electron microprobe and TEM analyses, respectively. Thin sections were cut approximately normal to bedding so that the planes of phyllosilicates

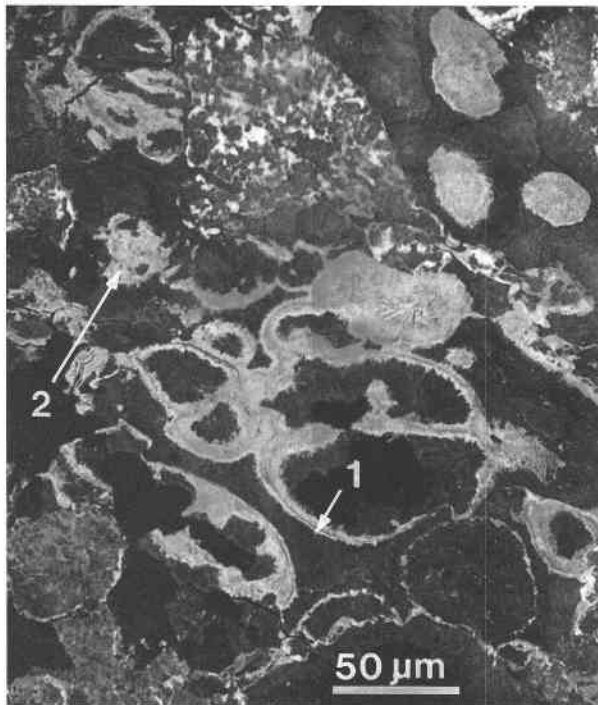


**FIGURE 1.** BSE image showing textural relation of ferroceladonite (1) and ferroaluminoceladonite (2). Ferroceladonite commonly occurs at vesicle walls, whereas ferroaluminoceladonite is intimately associated with chlorite in interiors of vesicles and as a replacement of glass shards.

would be preferentially oriented parallel to the electron beam for TEM observations. Thin sections were first examined by optical microscopy and SEM. Back-scattered electron (BSE) imaging and X-ray energy-dispersive spectrum (EDS) analyses were conducted with a Hitachi S-570 scanning electron microscope operated at 15 kV. Areas with large celadonite concentrations were then chosen for TEM observations. Ion-milled TEM specimens were prepared following the method described by Li et al. (1994). TEM observations and AEM analyses were obtained using a Philips CM12 scanning transmission electron microscope (STEM) fitted with a Kevex Quantum solid-state detector and computer system. The STEM was operated at an accelerating voltage of 120 kV and a beam current of  $\sim 10$  nA to obtain TEM images and SAED patterns. AEM quantitative chemical analyses were obtained using the standards muscovite (K, Al), clinchlore (Mg, Al, Fe), albite (Na, Al), fayalite (Fe), rhodonite (Mn, Fe, Ca), and titanite (Ti, Ca) to derive k ratios that were used to process EDS data, assuming the thin-foil approximation (Cliff and Lorimer 1975).

Electron microprobe analyses (EMPA) were obtained with a JEOL JXA 8600 electron microprobe using wavelength-dispersion methods. Operating conditions included a beam diameter up to about 5  $\mu\text{m}$  where optically homogeneous aggregates could be analyzed at this scale, 15 kV accelerating voltage, 20 nA probe current, with data

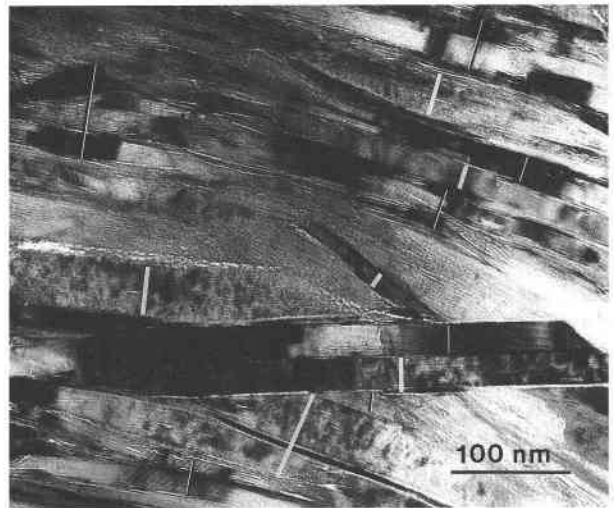


**FIGURE 2.** TEM image showing intergrown discrete packets of chlorite (thin white bars) and ferroaluminoceladonite (thick white bars), each a few hundred angstroms in thickness.

processed for ZAF corrections (Y.K. and M.W. Trinder, unpublished manuscript). Count times were reduced to minimize beam damage. Standards employed were natural albite for Na, potassium feldspar for K, natural hematite for Fe, synthetic wollastonite for Ca, and simple synthetic oxides for other elements. Spot analyses did not reveal detectable Ba or Sr.

### SEM and TEM observations

Fibrolamellar or tabular heulandite crystals occupy the sites of former glass shards. Some occur as spherical aggregates. Figure 1 is a BSE image showing the textural relations between ferroceladonite and ferroaluminoceladonite. Ferroceladonite occurs primarily as the outer lining of vesicles, which are approximately 25  $\mu\text{m}$  in diameter. It forms layers about 1–2  $\mu\text{m}$  thick of fibrolamellar crystallites oriented preferentially normal to vesicle walls. Ferroaluminoceladonite occurs intergrown with chlorite or other phyllosilicates in the interior regions of vesicles, and as a replacement of glass in some pumiceous shards. Interior regions of vesicles may also be occupied by chlorite or a heulandite-family zeolite or both. Other minerals observed by SEM include albite, quartz, titanite, apatite, pyrite, clastic feldspar, and detrital biotite.

Figure 2 is a TEM image showing intergrown packets of chlorite and ferroaluminoceladonite, each a few tens of nanometers in thickness. Although it is not as commonly associated with chlorite as is the ferroaluminoceladonite in vesicles, ferroceladonite at vesicle rims is sometimes observed to be intergrown with chlorite. Figure 3 is a lattice-fringe image of discrete packets of ferroceladonite and chlorite, showing that the chlorite contains 7  $\text{\AA}$  layers that are inferred to be berthierine. Although not shown, chlorite layers were occasionally observed to alternate with 10  $\text{\AA}$  layers, giving 24  $\text{\AA}$  pe-

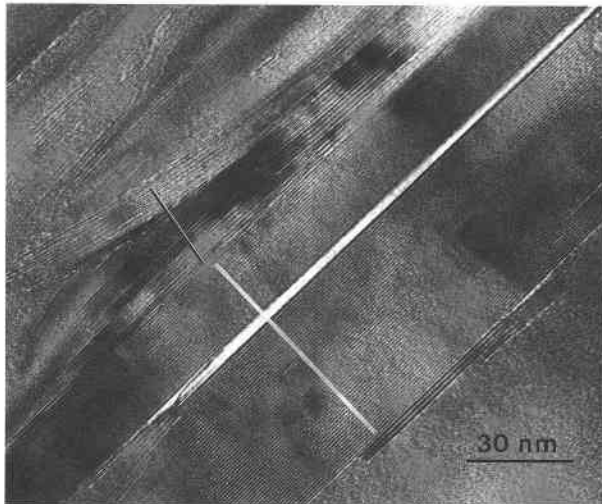


FIGURE 3. TEM (001) lattice-fringe image showing packets of ferroceldadonite (thick white bar) and mixed-layered chlorite and berthierine (thin white bar).

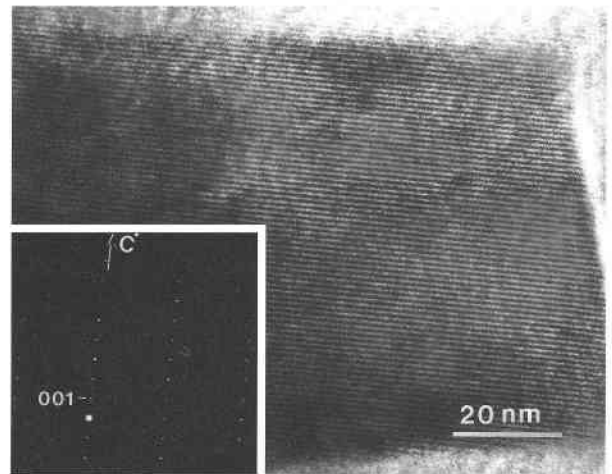


FIGURE 4. Lattice-fringe image of well-ordered ferroceldadonite. The inset electron diffraction pattern shows sharp  $0kl$  reflections consistent with the  $1M$  polytype.

riodicity. The individual layers were inferred to be smectite- or vermiculite-like, the 24 Å material being corrensite. Complex intergrowths and mixed-layering of such phyllosilicates is common in low-grade rocks (Peacor 1992). These textures show that electron microprobe analyses of such materials must almost invariably involve a mixture of two or more phases, and that macroscopic physical properties must be aggregate effects for such mixtures.

#### Physical and optical properties

Both ferroceldadonite and ferroaluminoceldadonite are dark blue-green in color, although bright blue-green and translucent in thin section. Hardnesses cannot be measured because of the small grain sizes, but are estimated to be 2–2.5 by analogy with other micas. The cleavage is perfect and no partings were observed. The calculated densities are 3.045(3) and 2.928(2) g/cm<sup>3</sup> for ferroceldadonite and ferroaluminoceldadonite, respectively.

Indices of refraction were measured on fine-grained aggregates consisting of flakes and granules little more than a few micrometers long with variable orientation and likely to contain intergrown chlorite. In spite of discernible pleochroism, it was not possible to measure separate refractive indices,  $\alpha$  and  $\gamma$ . Mean or aggregate refractive indices range from 1.625(5) to 1.640(5) (wavelength =  $\text{Na}_D$ ). Specific grains could not be identified as ferroceldadonite, ferroaluminoceldadonite, or mixtures, but the low and high values are assumed to correspond to ferroaluminoceldadonite and ferroceldadonite, respectively, on the basis of the expected relationship between refractive index and composition. The minerals are length slow, with  $Z \parallel$  cleavage, and are markedly pleochroic with  $Z =$  blue green,  $X =$  paler green,  $Z > X$ . The compatibility indices (Mandarino 1981) are 0.038 (excellent) and 0.001 (su-

perior) for ferroaluminoceldadonite and ferroceldadonite, respectively.

#### Crystallographic data

Single-crystal diffraction data were obtained by electron diffraction, with compositions of analyzed grains verified by AEM. Figure 4 shows a lattice-fringe image and a selected-area electron diffraction pattern of ferroceldadonite, that is also typical of ferroaluminoceldadonite. Non- $00l$  reflections (where  $k \neq 3n$ ) are sharp, indicating well-ordered, 10 Å periodicity consistent with the  $1M$  polytype. This is in agreement with results obtained for celadonite by previous workers using powder XRD (e.g., Yoder and Eugster 1955; Wise and Eugster 1964; Buckley et al. 1978; Odom 1984).

The powder diffractometer pattern was obtained from concentrates that contained both ferroceldadonite and ferroaluminoceldadonite and also gave peaks for admixed chlorite. Only one set of mica peaks was present, most peaks having half-height widths approximately equal to values expected for single minerals. This indicates that lattice parameters of ferroceldadonite and ferroaluminoceldadonite are approximately equal. However, a few peaks were slightly broadened, which is consistent with small differences in lattice parameters. Powder diffraction data for the composite ferroceldadonite-ferroaluminoceldadonite sample are listed in Table 1, with data for celadonite for comparison. Cell parameters were refined by least-squares, giving rise to the values  $a = 5.270(5)$ ,  $b = 9.106(7)$ ,  $c = 10.125(8)$  Å,  $\beta = 100.27(14)^\circ$ ,  $V = 478.1(4)$  Å<sup>3</sup> for which  $Z = 2$  for the composite ferroceldadonite-ferroaluminoceldadonite sample. In comparison with lattice parameters of celadonite (Wise and Eugster 1964),  $a$  and  $b$  are slightly larger, and  $c$  and  $\beta$  slightly smaller.

**TABLE 1.** Powder XRD data for a composite ferroceldadonite-ferroaluminoceldadonite sample and for celadonite

| Ferroceldadonite-ferroaluminoceldadonite |                |                 |            | Celadonite*    |                 |          |            |
|--|----------------|-----------------|------------|----------------|-----------------|----------|------------|
| <i>l</i>                                 | <i>d</i> (obs) | <i>d</i> (calc) | <i>hkl</i> | <i>d</i> (obs) | <i>d</i> (calc) | <i>l</i> | <i>hkl</i> |
| 40                                       | 10.00          | 9.96            | 001        | 9.97           | 9.94            | 47       | 001        |
| 32                                       | 4.55           | 4.55            | 020        | 4.53           | 4.53            | 85       | 020        |
| 30                                       | 4.37           | 4.37            | 111        | 4.35           | 4.36            | 42       | 111        |
| 35                                       | 4.14           | 4.14            | 021        | 4.14           | 4.123           | 37       | 021        |
| 52                                       | 3.65           | 3.63            | 112        | 3.635          | 3.638           | 80       | 112        |
| 86                                       | 3.358          | 3.361           | 022        | 3.35           | 3.349           | 60       | 022        |
| 100                                      | 3.321          | 3.321           | 003        | 3.318          | 3.314           | 70       | 003        |
| 60                                       | 3.090          | 3.111           | 112        | 3.087          | 3.081           | 80       | 112        |
| 40B**                                    | 2.91           | 2.896           | 113        | 2.90           | 2.901           | 10B      | 113        |
| 48                                       | 2.671          | 2.683           | 023        | 2.678          | 2.675           | 75       | 023        |
| 40                                       | 2.607          | 2.620           | 130        | 2.604          | 2.605           | 70       | 130        |
| 50                                       | 2.584          | 2.592           | 131        | 2.580          | 2.581           | 100      | 131        |
| 35B                                      | 2.41           | 2.410           | 132        | 2.402          | 2.404           | 75       | 132        |
|  |                | 2.407           | 201        |                |                 |          |            |
|  |                |                 |            | 2.264          | 2.265           | 20       | 040        |
|  |                |                 |            | 2.209          | 2.208           | 25       | 041        |
| 33                                       | 2.155          | 2.153           | 133        | 2.148          | 2.250           | 31       | 133        |
|  |                | 2.148           | 202        |                | 2.125           | 31       | 202        |
|  |                |                 |            | 2.092          | 1.988           | 10       | 005        |
| 40                                       | 1.660          | 1.661           | 006        |                |                 |          |            |
|  |                | 1.660           | 135        |                |                 |          |            |
|  |                |                 |            | 1.65           | 1.665           | 15B      | 151        |
| 40                                       | 1.519          | 1.520           | 331        | 1.509          | 1.510           | 60       | 060        |
|  |                | 1.518           | 060        |                |                 |          |            |

\* Wise and Eugster 1964,  $a = 5.23(2)$ ,  $b = 9.06(1)$ ,  $c = 10.13(2)$  Å,  $\beta = 100.55(10)^\circ$

\*\*B = broad peak.

## CHEMICAL COMPOSITIONS

### AEM data

Formulas (Tables 2 and 3) were calculated by normalization of AEM data to a dioctahedral mica formula with the sum of octahedrally and tetrahedrally coordinated cations equal to 12, the  $\text{Fe}^{3+}:\text{Fe}^{2+}$  ratio then being determined by charge balance. This method of normalization was chosen because the collective data (see below) imply that, by analogy with celadonite, both ferroceldadonite and ferroaluminoceldadonite are dioctahedral. Furthermore, the value of  $d_{060}$  is a sensitive indicator of octahedral occupancy, and the observed value (1.519 Å) is firmly in the

range for dioctahedral phyllosilicates (Moore and Reynolds 1989). In addition, using the relations of Radoslovich and Norrish (1962) for cell parameters vs. tetrahedral Al occupancy, a value of  $b = 9.107$  Å, on the basis of the calculated O-T-O angle, was calculated; it is nearly identical to that obtained from the powder XRD pattern (9.106 Å), implying that the normalized tetrahedrally coordinated Si, Al occupancies, and assumptions regarding the dioctahedral character are therefore accurate.

Columns 13 and 14 of Tables 2 and 3 show the numbers of cations that were obtained by normalizing average ferroceldadonite and ferroaluminoceldadonite analyses assuming there were 12.2 and 12.5 tetrahedral plus octahedral cations, respectively. This corresponds to 10% and 25% trioctahedral components, respectively. The results show that for only 10% calculated trioctahedral occupancy, the number of Si atoms pfu exceeds the structurally possible limit of eight. Furthermore, the number of Si atoms far exceeds this limit, and the number of K atoms exceeds its possible limit of two for the formulas on the basis of 25% trioctahedral character. These calculations confirm that ferroceldadonite and ferroaluminoceldadonite are largely, if not entirely, dioctahedral in nature, and that the normalized formulas given in Tables 2 and 3 realistically define their compositions. However, we cannot rule out the possibility of small (approximately < 10%) trioctahedral components and  $\text{Fe}^{3+}:\text{Fe}^{2+}$  ratios slightly different from those given in Tables 2 and 3. The close approach of the K value to the ideal mica content of two, and of Si to the ideal celadonite value of eight, is noteworthy.

### Range of solid solution for the celadonite family

The 1978 AIPEA Nomenclature Committee recommended that celadonite be defined as "a dioctahedral mica of ideal composition,  $\text{KMgFe}^{3+}\text{Si}_4\text{O}_{10}(\text{OH})_2$ , but allowing a tetrahedral Al range of about 0.0 to 0.2 atoms per formula unit (pfu)" (Bailey 1980). Other workers have reported tetrahedral Al contents for celadonite up to and occasionally exceeding 0.3 pfu (Weaver and Pollard

**TABLE 2.** Normalized AEM data for ferroceldadonite in sample 26049 from South Island, New Zealand\*

|  | 1     | 2      | 3     | 4     | 5     | 6     | 7     | 8     | 9     | 10    | 11    | 12    | Average | 13    | 14    |
|--|-------|--------|-------|-------|-------|-------|-------|-------|-------|-------|-------|-------|---------|-------|-------|
| Si   | 7.93  | 7.94   | 7.92  | 7.99  | 7.93  | 7.83  | 7.86  | 8.00  | 7.91  | 8.00  | 7.83  | 7.95  | 7.92    | 8.05  | 8.25  |
| <sup>27</sup> Al   | 0.07  | 0.06   | 0.08  | 0.01  | 0.07  | 0.17  | 0.14  | —     | 0.09  | —     | 0.17  | 0.05  | 0.08    | -0.05 | -0.25 |
| <sup>29</sup> Al   | 0.46  | 0.62   | 0.52  | 0.38  | 0.64  | 0.69  | 0.65  | 0.69  | 0.79  | 0.41  | 0.66  | 0.45  | 0.58    | 0.67  | 0.69  |
| Ti   | 0.04  | n.d.** | 0.13  | 0.13  | n.d.  | 0.03  | 0.08  | 0.08  | n.d.  | n.d.  | n.d.  | n.d.  | 0.04    | 0.04  | 0.04  |
| Fe <sup>3+</sup>   | 1.59  | 1.45   | 1.30  | 1.40  | 1.43  | 1.45  | 1.50  | 1.24  | 1.40  | 1.64  | 1.67  | 1.70  | 1.49    | 0.94  | 0.47  |
| Fe <sup>2+</sup>   | 1.17  | 1.56   | 1.60  | 1.58  | 1.32  | 1.03  | 1.19  | 1.26  | 1.28  | 1.21  | 1.04  | 1.12  | 1.27    | 1.87  | 2.41  |
| Mg   | 0.70  | 0.29   | 0.36  | 0.37  | 0.61  | 0.75  | 0.51  | 0.68  | 0.46  | 0.66  | 0.53  | 0.65  | 0.55    | 0.56  | 0.57  |
| Mn   | 0.04  | 0.08   | 0.09  | 0.14  | n.d.  | 0.05  | 0.07  | 0.05  | 0.07  | 0.08  | 0.10  | 0.08  | 0.07    | 0.07  | 0.07  |
| K  | 1.94  | 1.99   | 2.00  | 1.97  | 2.00  | 1.97  | 1.83  | 1.91  | 1.90  | 1.95  | 1.84  | 1.90  | 1.93    | 1.96  | 2.01  |
| Total cations  | 13.94 | 13.99  | 14.00 | 13.97 | 14.00 | 13.97 | 13.83 | 13.91 | 13.90 | 13.95 | 13.84 | 13.90 | 13.93   | 14.16 | 14.51 |
| <sup>27</sup> Al/( <sup>27</sup> Al + Fe <sup>3+</sup> ) | 0.22  | 0.23   | 0.29  | 0.21  | 0.31  | 0.32  | 0.30  | 0.36  | 0.36  | 0.20  | 0.28  | 0.21  | 0.28    | 0.42  | 0.59  |
| Mg/(Mg + Fe <sup>2+</sup> )                              | 0.37  | 0.16   | 0.18  | 0.19  | 0.32  | 0.42  | 0.30  | 0.35  | 0.27  | 0.35  | 0.34  | 0.37  | 0.30    | 0.23  | 0.19  |

\* Analyses 1–12, 13, and 14 are calculated on the basis of 12, 12.2, and 12.5 tetrahedral and octahedral cations, respectively, and Fe<sup>3+</sup> is calculated from charge balance. Two standard deviations on the basis of calculating statistics are 0.07–0.09 pfu for Si, 0.03–0.05 pfu for Al, 0.01 pfu for Ti, 0.10–0.20 pfu for Fe, 0.02–0.04 pfu for Mg, 0.01–0.02 pfu for Mn, 0.06–0.13 pfu for K.

\*\* n.d. = not detectable.

**TABLE 3.** Normalized AEM data for ferroaluminoceladonite in sample 26049 from South Island, New Zealand\*

|  | 1      | 2     | 3     | 4     | 5     | 6     | 7     | 8     | 9     | 10    | 11    | 12    | Average | 13    | 14    |
|--|--------|-------|-------|-------|-------|-------|-------|-------|-------|-------|-------|-------|---------|-------|-------|
| Si   | 7.79   | 8.00  | 7.92  | 8.00  | 8.00  | 7.90  | 7.98  | 7.88  | 7.84  | 7.88  | 7.93  | 7.95  | 7.92    | 8.05  | 8.25  |
| <sup>4</sup> Al  | 0.21   | 0.00  | 0.08  | 0.00  | 0.00  | 0.10  | 0.02  | 0.12  | 0.16  | 0.12  | 0.07  | 0.05  | 0.08    | -0.05 | -0.25 |
| <sup>6</sup> Al  | 2.06   | 1.52  | 1.78  | 1.51  | 1.44  | 1.51  | 1.61  | 1.40  | 1.65  | 1.72  | 1.52  | 1.61  | 1.61    | 1.72  | 1.76  |
| Ti   | n.d.** | 0.06  | 0.06  | n.d.  | n.d.  | 0.06  | n.d.  | 0.12  | 0.07  | 0.03  | 0.04  | 0.08  | 0.04    | 0.04  | 0.04  |
| Fe <sup>3+</sup>                                       | 0.21   | 0.38  | 0.23  | 0.59  | 0.57  | 0.53  | 0.47  | 0.63  | 0.60  | 0.45  | 0.49  | 0.43  | 0.48    | —     | —     |
| Fe <sup>2+</sup>                                       | 0.97   | 1.35  | 1.35  | 1.13  | 1.31  | 1.03  | 1.15  | 1.12  | 1.02  | 1.10  | 1.34  | 1.13  | 1.16    | 1.67  | 1.71  |
| Mg   | 0.67   | 0.64  | 0.58  | 0.63  | 0.57  | 0.82  | 0.73  | 0.61  | 0.60  | 0.70  | 0.57  | 0.67  | 0.65    | 0.66  | 0.68  |
| Mn   | 0.09   | 0.05  | n.d.  | 0.14  | 0.11  | 0.05  | 0.04  | 0.12  | 0.06  | n.d.  | 0.04  | 0.08  | 0.06    | 0.06  | 0.06  |
| K  | 1.94   | 1.98  | 1.95  | 1.90  | 1.99  | 1.94  | 1.90  | 1.85  | 1.77  | 1.89  | 1.98  | 1.85  | 1.91    | 1.94  | 1.99  |
| Total cations  | 13.94  | 13.98 | 13.95 | 13.90 | 13.99 | 13.94 | 13.90 | 13.85 | 13.77 | 13.89 | 13.98 | 13.85 | 13.91   | 14.14 | 14.49 |
| <sup>6</sup> Al/( <sup>6</sup> Al + Fe <sup>3+</sup> ) | 0.91   | 0.80  | 0.89  | 0.72  | 0.72  | 0.74  | 0.77  | 0.69  | 0.73  | 0.79  | 0.76  | 0.79  | 0.77    | —     | —     |
| Mg/(Mg + Fe <sup>2+</sup> )                            | 0.41   | 0.32  | 0.30  | 0.36  | 0.30  | 0.44  | 0.39  | 0.35  | 0.37  | 0.39  | 0.30  | 0.37  | 0.36    | 0.28  | 0.28  |

\* Analyses 1–12, 13, and 14 are calculated on the basis of 12, 12.2, and 12.5 tetrahedral and octahedral cations, respectively, and Fe<sup>3+</sup> is calculated from charge balance. Two standard deviations on the basis of calculating statistics are 0.07–0.09 pfu for Si, 0.03–0.07 pfu for Al, 0.01 pfu for Ti, 0.08–0.15 pfu for Fe, 0.02–0.06 pfu for Mg, 0.01–0.02 pfu for Mn, 0.06–0.13 pfu for K.

\*\* n.d. = not detectable.

1975; Odom 1984), although the purity of some of the samples was not made clear.

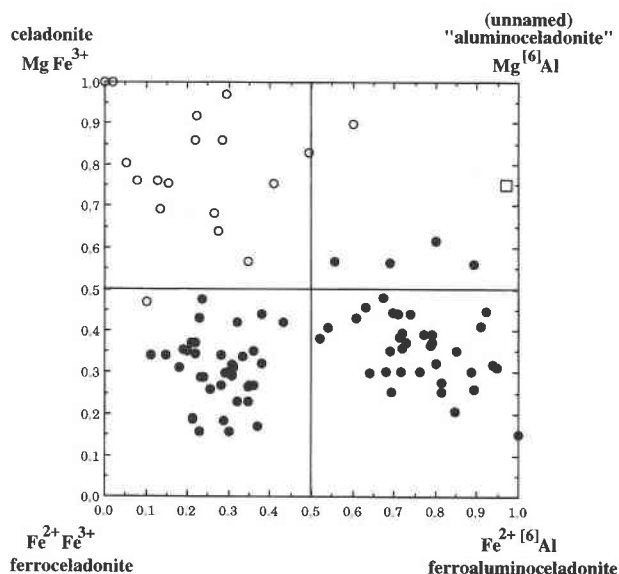
The composition of the octahedral layer varies widely in celadonite. Buckley et al. (1978) stated that the amounts of Fe<sup>3+</sup> and <sup>6</sup>Al vary considerably in a reciprocal manner. Compilations of celadonite analyses by Foster (1969), Weaver and Pollard (1975) following Wise and Eugster (1964), and Buckley et al. (1978) mostly show octahedral Fe<sup>3+</sup> > <sup>6</sup>Al, but some analyses are listed with subequal <sup>6</sup>Al and Fe<sup>3+</sup>, and some with predominant <sup>6</sup>Al, as with the mineral described as Mg-Al-celadonite by Seifert (1968). Buckley et al. (1978) reported a relatively constant octahedral R<sup>3+</sup>:R<sup>2+</sup> ratio of approximately 1:1 and a fairly constant Fe<sup>3+</sup>:Fe<sup>2+</sup> ratio of approximately 2.6:1 for celadonite.

Figure 5 is a plot of the octahedral cation contents of the celadonite-family minerals of this study, with data of Odin et al. (1988) for celadonite and Seifert (1968) for "Mg-Al-celadonite" for comparison. Assuming that the latter data represent pure phases, and bearing in mind the synthesis data, the plot suggests that there is nearly complete solid solution among all four end-members of the family. Those analyses plotting in the fields with dominant octahedral occupancies of the ideal end-member Fe<sup>2+</sup>Fe<sup>3+</sup> and Fe<sup>2+</sup><sup>6</sup>Al correspond to the new minerals ferroceladonite and ferroaluminoceladonite, respectively. Although some analyses fall within the field with end-member Mg<sup>6</sup>Al, they do so only marginally, and we do not propose that they be used to define the mineral in which this component is dominant.

### Electron microprobe data

Electron microprobe analyses of the sample of this study were given by Boles and Coombs (1975) and provided evidence of intermixing with chlorite. More than 60 additional analyses have been obtained, including analyses of both bright blue-green celadonite and olive-green aggregates suspected of containing substantial chlorite. The K and Si contents of the electron microprobe analyses are plotted in Figure 6, for which all analyses were normalized to a celadonite-family formula with a total of 12 octahedral and tetrahedral cations, even where contamination with chlorite was likely. There is a tightly constrained linear correlation from a point representing average "chlorite" in the rock, with only 0.04% K<sub>2</sub>O, to near end-member celadonite-family minerals. This confirms that the microprobe analyses are of mixtures of celadonite-family minerals and chlorite. It confirms the general effect of submicrometer intergrowths on electron microprobe analyses, even where materials appear to be optically homogeneous.

Figure 7 demonstrates that with the celadonite normalization adopted, a few of the electron microprobe analyses plot in the ferroceladonite and Mg<sup>6</sup>Al fields of the celadonite-family quadrilateral, but that most plot in



**FIGURE 5.** Plot of relative numbers of octahedral cations of celadonite-family minerals from AEM analyses of this study (solid circles), celadonite of Odin (1988) (open circles), and "Mg-Al-celadonite" of Seifert (1968) (open square).

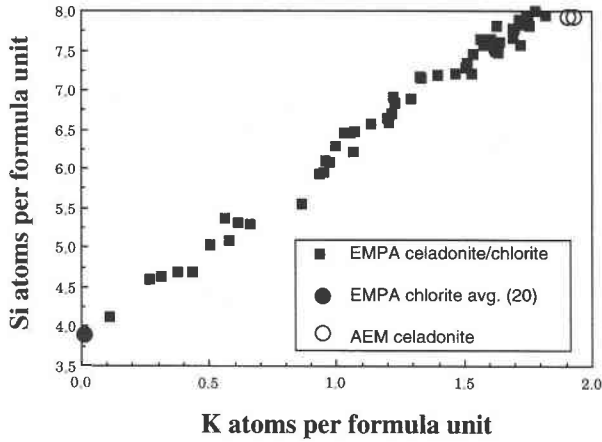


**FIGURE 6.** Plot of numbers of K and Si atoms pfu for formulas derived from electron microprobe analyses of mixtures with variable proportions of chlorite containing probable berthierine and corrensite mixed-layers and of celadonite-family minerals in sample OU 26049. Formulas normalized to 12 tetrahedral + octahedral cations.

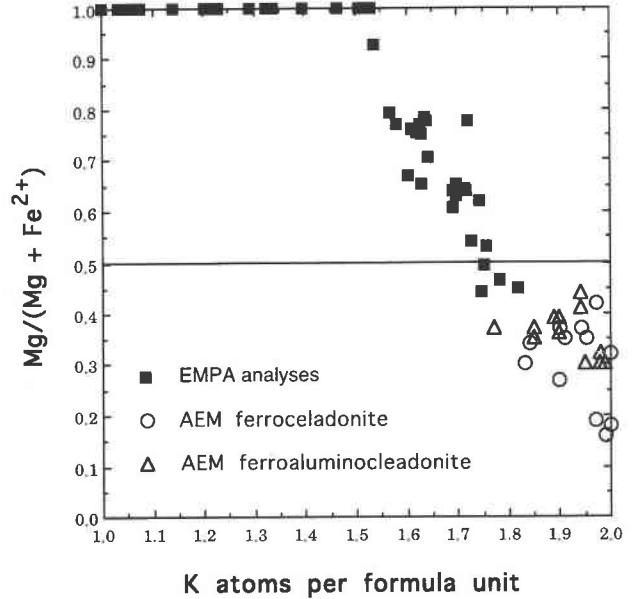


**FIGURE 8.**  $Mg/(Mg + Fe^{2+})$  vs. K cation contents for electron microprobe analyses of celadonite-family minerals submicroscopically intergrown with "chlorite" and for AEM analyses of homogeneous packets of ferroceldonite and ferroaluminoceldonite as verified by TEM, normalized to 12 tetrahedral + octahedral cations and 22 O atoms. The electron microprobe analyses cover a range of  $^{60}Al/(^{60}Al + Fe^{3+})$  values. Analyses that plot below the horizontal line fall in the ferroceldonite or ferroaluminoceldonite fields of the celadonite quadrilateral.

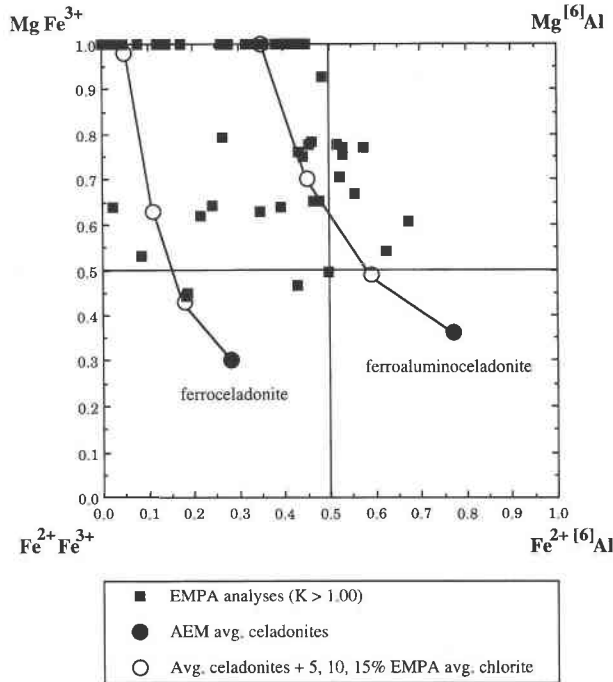


**FIGURE 7.** Octahedral cation contents for electron microprobe analyses of celadonite-family minerals submicroscopically intergrown with "chlorite" and of average AEM analyses of homogeneous packets of ferroceldonite and ferroaluminoceldonite in the same rock; these latter analyses are joined to points corresponding to the addition of 5, 10, and 15% of average "chlorite" as analyzed by the electron microprobe. All analyses normalized to 12 tetrahedral + octahedral cations and 22 O atoms; only analyses with  $K \geq 1$  pfu are plotted.

the celadonite field. However, it is also demonstrated in Figure 7 that projection points for average analyzed ferroceldonite and average ferroaluminoceldonite contaminated by only 5–10% analyzed chlorite are displaced into the celadonite field, and 15% chlorite takes them to the upper limit of that field. The negative slope of the trend lines results from the fact that contamination of a Si-rich celadonite mineral by Si-poor chlorite causes increasing amounts of Al to be required to fill nominal tetrahedral sites with increasing nominal  $Fe^{2+}$  relative to  $Fe^{3+}$  to maintain charge balance. The observed concentration of projected points for electron microprobe analyses of celadonite-family minerals in OU 26049 toward the upper left quadrant results from this effect. We interpret analyses plotting close to the ferroaluminoceldonite field as ferroaluminoceldonite with minor chlorite. With the inevitability of microprobe beam interaction with phases shown by TEM to be multiple phases on a size scale less than the microprobe beam, EMPA analyses do not adequately characterize single phases of these minerals, but AEM data may (Li et al. 1996). Nevertheless, the properly interpreted microprobe analyses support the formulas for both ferroceldonite and ferroaluminoceldonite.

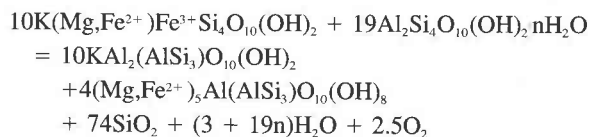
Figure 8 illustrates a negative correlation between  $Mg/(Mg + Fe^{2+})$  and K, as normalized from EMPA analyses of celadonite-family minerals contaminated by chlorite, irrespective of  $^{60}Al/(^{60}Al + Fe^{3+})$  values. For the

compositions concerned, and where the amount of chlorite contaminant is such that K is less than approximately 1.5 (and Si less than approximately 7.3), the celadonite normalization procedure that was adopted requires all Fe to be Fe<sup>3+</sup>, so that Mg/(Mg + Fe<sup>2+</sup>) = 1. Where the Mg/(Mg + Fe<sup>2+</sup>) of chlorite reaches 1, total cation charges are less than 44, permitting less than 22 O atoms in the nominal formula. Whereas the normalization procedure is believed to give reasonable Fe<sup>2+</sup>:Fe<sup>3+</sup> ratios and hence Mg:(Mg + Fe<sup>2+</sup>) ratios, for uncontaminated celadonite-family minerals as with the AEM analyses, it does not do so for celadonite-chlorite mixtures.

### PARAGENESIS

Wise and Eugster (1964) pointed out that celadonite is widespread in the zeolite facies and in some assemblages with prehnite. It has also been reported from the lawsonite-albite-chlorite facies (Landis 1974), but not from the greenschist facies. This appears to contradict the results of Wise and Eugster (1964) that at fluid pressures of 2 kbar, the MgFe<sup>3+</sup> (celadonite) end-member is stable up to temperatures of about 400–425 °C depending on *f*<sub>O<sub>2</sub></sub>. At this point it breaks down reversibly to ferritribotite + liquid or to ferriphlogopite + ferrisanidine together with quartz and H<sub>2</sub>O vapor. Wise and Eugster suggested that natural celadonite is lost during progressive metamorphism long before its upper stability limit is reached as a result of reactions with hydrous aluminous silicates.

An equation can be written as follows for reaction between celadonite-ferroceladonite solid solutions and aluminous smectite to yield a muscovite component of illite or phengite and a chlorite component:



Similar equations can be written for reactions between MgAl celadonite-ferroaluminoceladonite solid solutions and aluminous smectite components (not involving change in oxidation state), with kandites instead of smectite, or, as suggested by Coombs et al. (1959), for reaction between celadonite-family minerals and a calcium zeolite, such as laumontite or heulandite, in this case yielding pumpellyite as well as chlorite and white mica.

All these reactions result in substantial dehydration and release of silica. Where an Fe<sup>3+</sup>-bearing member of the celadonite family is involved, the oxygen content of the reactants is reduced to form Fe<sup>2+</sup> in chlorite. Thus it is clear that such reactions, not necessarily under closed-system conditions, are to be expected with progressive very low-grade metamorphism, with celadonite-aluminous clay mineral ± Calcium zeolite being an alternative lower grade assemblage compared with muscovite-chlorite-quartz ± pumpellyite as in the prehnite-pumpellyite facies. Both sets of assemblages and the detailed compositions of the phases are sensitive to *P*<sub>H<sub>2</sub>O</sub> and *f*<sub>O<sub>2</sub></sub>. The

gross dependence of chlorite compositions on *f*<sub>O<sub>2</sub></sub> in diagenesis and very low-grade metamorphism has recently been emphasized by Coombs et al. (1996), as has the Mg:Fe ratio in saponites by Andrews (1980). The occurrence of pyrite, berthierine, and trace siderite in sample OU 26049 is compatible with relatively reducing conditions, allowing Fe<sup>2+</sup> as well as Fe<sup>3+</sup> in the celadonite minerals.

### ACKNOWLEDGMENTS

We thank Eric Essene, Howard Evans, and Malcolm Ross for their reviews. This study was supported by NSF grant EAR-91-04565 to D.R.P. and by research contracts from the New Zealand Foundation for Research, Science and Technology to D.S.C. The STEM used in this study was acquired under grant no. EAR-87-08276, and the SEM under grant no. BSR-83-14092 from the National Science Foundation. The electron microprobe was purchased in part with grants from the former New Zealand University Grants Committee and the Science Lottery Grants Board. D.S.C. and Y.K. are grateful to M.W. Trinder for microprobe programming and maintenance. Contribution No. 505 from the Mineralogical Laboratory, Department of Geological Sciences, University of Michigan.

### REFERENCES CITED

- Andrews, A.J. (1980) Saponite and celadonite in layer 2 basalts, DSDP Leg 37. *Contributions to Mineralogy and Petrology*, 73, 323–340.
- Bailey, S.W. (1980) Summary of recommendations of ALPEA Nomenclature Committee. *Clay Minerals*, 15, 85–93.
- Boles, J.R. (1972) Composition, optical properties, cell dimensions, and thermal stability of some heulandite group minerals. *American Mineralogist*, 57, 1463–1493.
- Boles, J.R. and Coombs, D.S. (1975) Mineral reactions in zeolitic Triassic tuff, Hokonui Hills, New Zealand. *Geological Society of America Bulletin*, 86, 163–173.
- Buckley, H.A., Bevan, J.C., Brown, K.M., Johnson, L.R., and Farmer, V.C. (1978) Glauconite and celadonite: two separate mineral species. *Mineralogical Magazine*, 42, 373–382.
- Cathelineau, M. and Izquierdo, G. (1988) Temperature-composition relationships of authigenic micaceous minerals in the Los Azufres geothermal system. *Contributions to Mineralogy and Petrology*, 100, 418–428.
- Cliff, G. and Lorimer, G.W. (1975) The quantitative analysis of thin specimens. *Journal of Microscopy*, 103, 203–207.
- Coombs, D.S. (1954) The nature and alteration of some Triassic sediments from Southland, New Zealand. *Transactions of the Royal Society of New Zealand*, 82, 65–109.
- Coombs, D.S., Ellis, A.J., Fyfe, W.S., and Taylor, A.M. (1959) The zeolite facies, with comments on the interpretation of hydrothermal syntheses. *Geochimica et Cosmochimica Acta*, 17, 53–107.
- Coombs, D.S., Kawachi, Y., and Ford, P.B. (1996) Porphyroblastic mangaxinite metapelagites with incipient garnet in prehnite-pumpellyite facies, near Meyers Pass, Torlesse Terrane, New Zealand. *Journal of Metamorphic Petrology*, 14, 125–142.
- Foster, M.D. (1969) Studies of celadonite and glauconite. U.S. Geological Survey Professional Paper, 614-F, 1–17.
- Hendricks, S.B. and Ross, C.S. (1941) Chemical composition and genesis of glauconite and celadonite. *American Mineralogist*, 12, 683–708.
- Honda, S. and Muffler, L.J.P. (1970) Hydrothermal alteration in core from Research Drill Hole Y-1, Upper Geyser Basin, Yellowstone National Park, Wyoming. *American Mineralogist*, 55, 1714–1737.
- Landis, C.A. (1974) Stratigraphy, lithology, structure, and metamorphism of Permian, Triassic, and Tertiary rocks between the Mararoa River and Mount Snowdon, western Southland, New Zealand. *Journal of the Royal Society of New Zealand*, 4, 229–251.
- Li, G., Peacor, D.R., Merriman, R.J., Roberts, B., and van der Pluijm, B.A. (1994) TEM and AEM constraints on the origin and significance of chlorite-mica stacks in slates: an example from central Wales, U.K. *Journal of Structural Geology*, 16, 1139–1157.
- Li, G., Peacor, D.R., Coombs, D.S., and Kawachi, Y. (1996) TEM/AEM characterization of fine-grained clay minerals in very low-grade rocks:

- evaluation of contamination by EMPA involving celadonite family minerals. In G.W. Bailey, J.M. Corbett, R.V.W. Dimlich, J.R. Michael and N.J. Zaluzac, Eds., *Proceedings of Microscopy and Microanalysis*, p 694–695. San Francisco Press, California.
- Loveland, P.J. and Bendelow, V.C. (1984) Celadonite-aluminous glauconite: An example from the Lake District, U.K. *Mineralogical Magazine*, 48, 113–117.
- Mandarino, J.A. (1981) The Gladstone-Dale relationship: Part IV. The compatibility concept and its application. *Canadian Mineralogist*, 19, 441–450.
- Moore, D.M. and Reynolds, R.C. Jr. (1989) *X-ray Diffraction and the Identification and Analysis of Clay Minerals*, 332 p. Oxford University Press, New York.
- Odin, G.S., Desprairies, A., Fullagar, P.D., Bellon, H., Decarreau, A., Frohlich, F., and Zelvelder, M. (1988) Nature and geological significance of celadonite. in *Green Marine Clays*, G. S. Odin, Ed., *Developments in Sedimentology* 45, 445 p. Elsevier, New York.
- Odom, E. (1984) Glauconite and celadonite minerals. In *Mineralogical Society of America Reviews in Mineralogy*, 13, 545–572.
- Peacor, D.R. (1992) Diagenesis and low-grade metamorphism of shales and slates. In *Mineralogical Society of America Reviews in Mineralogy*, 27, 335–380.
- Radoslovich, E.W. and Norrish, K. (1962) The cell dimensions and symmetry of layer-lattice silicates. I. Some structural considerations. *American Mineralogist*, 47, 599–616.
- Schaller, W.T. (1950) An interpretation of the composition of high-silica sericites. *Mineralogical Magazine*, 29, 406–415.
- Seifert, F. (1968) X-ray powder data for Mg-Al celadonite (Jeucophyllite) from Barcza, Poland. *Contributions to Mineralogy and Petrology*, 19, 93–96.
- Velde, B. (1972) Celadonite mica: solid solution and stability. *Contributions to Mineralogy and Petrology*, 37, 235–247.
- Weaver, C.E. and Pollard, L.D. (1975) *The Chemistry of Clay Minerals*. Elsevier Scientific Publication Co., New York.
- Wise, W.S. and Eugster, H.P. (1964) Celadonite: synthesis, thermal stability and occurrence. *American Mineralogist*, 49, 1031–1083.
- Yoder, H.S. and Eugster, H.P. (1955) Synthetic and natural muscovites. *Geochimica et Cosmochimica Acta*, 8, 225–280.

MANUSCRIPT RECEIVED JULY 11, 1996

MANUSCRIPT ACCEPTED JANUARY 31, 1997